Theory and simulations on strong pinning of vortex lines by nanoparticles

A. E. Koshelev and A. B. Kolton

Phys. Rev. B **84**, 104528 — Published 30 September 2011

DOI: 10.1103/PhysRevB.84.104528

Theory and simulations on strong pinning of vortex lines by nanoparticles

A. E. Koshelev
Materials Science Division, Argonne National Laboratory, Argonne, Illinois 60439

A. B. Kolton
CONICET, Centro Atómico Bariloche, 8400 S. C. de Bariloche, Argentina
(Dated: August 26, 2011)

Pinning of vortex lines by array of nanoparticles embedded inside superconductors became the most efficient practical way to achieve high critical currents. In this situation pinning occurs via trapping of the vortex-line segments and the critical current is determined by the typical length of trapped segment. To verify analytical estimates and develop a quantitative description of strong pinning, we numerically simulated isolated vortex lines driven through array of nanoparticles. We found that the critical force grows roughly as a square root of the pin density and it is strongly suppressed by thermal noise. The configurations of pinned lines are strongly anisotropic, displacements in the drive directions are much larger than in the transverse direction. Moreover, we found that the roughening index for the longitudinal displacements exceeds one. This indicates that the local stresses in the critical region increase with the total line length and the elastic description breaks down in the thermodynamic limit. Thermal noise reduces the anisotropy of displacements in the critical regions and straightens the lines.

I. INTRODUCTION

Introducing large-size nanoparticles of different shapes emerged as the best practical way to improve current performance of high-temperature superconductors. While in the first superconducting cables the critical currents were limited by weak links, in the second generation superconducting wires based on aligned $YBa_2Cu_3O_7$ (YBCO) films this problem was mostly resolved and critical currents are determined by vortex pinning. An impressive progress has been made to enhance critical currents in these films using both isotropic[1–7] and columnar[8–10] inclusions. In spite of this progress, understanding of strong pinning mechanisms is far from satisfactory. Theoretical estimates describing pinning of the vortex lines by array of strong pins at low temperatures were elaborated by Ovchinnikov and Ivlev.[11] This theory was applied to describe behavior of the critical currents in the real YBCO films in Refs. 12 and 13. In particular, frequently observed power-law decay of the critical current as function of the magnetic field with power slightly larger then 1/2 is naturally explained by this theory. More recently, it was also argued that strong pins of unknown origin determine critical currents at low magnetic fields in several iron-pnictide compounds.[14] It is not clear, however, to what extent available qualitative estimates describe the real situation. Due to the obvious importance of strong pinning by large-size inclusions for real superconducting materials, it is desirable to elaborate a quantitative theory describing pinning in such situation. Moreover, the very important issue of pinning suppression by thermal fluctuations does not have any theoretical description in the strong-pinning regime.

In this paper we consider pinning of vortex lines in a superconductor containing insulating inclusions with lateral sizes larger than the coherence length. We focus on pinning of individual vortex lines corresponding to small magnetic fields. Pinning occurs via trapping of finite-size segments of a vortex line[11] with the typical length L, as illustrated in Fig. 1. The critical current is determined by the length of trapped segment L and the pin-breaking force F_p,

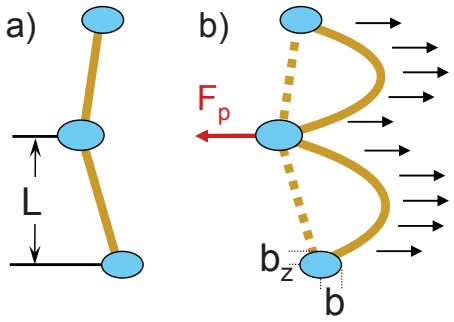

FIG. 1. Vortex line trapped by strong pinning centers at zero (a) and finite (b) current.

$$\frac{\Phi_0}{c} j_c \approx \frac{F_p}{L}. \tag{1}$$

Therefore in the strong-pinning regime the critical-current problem is mostly reduced to evaluation of the trapped-segment length L. In general, trapping of the vortex lines is a complicated dynamic process controlled by the competition between the pinning energy, line tension, and intervortex interactions. Different approaches may be used to evaluate the trapped-segment length. One can assume that the pinning center always grabs a piece of the vortex line when it is energetically favorable. This assumption implies that thermal fluctuations facilitate local equilibration. In this case parameters of trapped configurations can be obtained from the energy-balance estimates. We will call this type of trapping the

equilibrium regime. This energy-balance consideration determines trapped configurations of static vortex lines prepared by cooling in finite magnetic field. However, such consideration is not applicable to the more typical dynamic scenario when moving lines are trapped after the driving force is slowly reduced down to the critical value. In this case the line motion close to the critical force is a continuous trapping-detrapping process limited by local instabilities. The driven vortex can be captured when the line either directly collides with the strong pin or passes sufficiently close to it. In the second case trapping may occur due to the long-range pin-vortex interaction as a result of local instability.[11] The line remains trapped until the force acting from the pin does not exceed the pin-breaking force. When the line finally stops, the pinned configuration is expected to be very anisotropic because the transverse pin-to-pin displacements which are determined by trapping events are much smaller than the longitudinal displacements limited by the pin-breaking criteria.

To develop a quantitative picture and verify analytical estimates, we explore in this paper pinning of the vortex lines by nanoparticles with extensive numerical simulations. We study the dependence of the critical force on the density of pins, statistical properties of trapped lines including average values and distributions of trapping length and pin-to-pin displacements. We study long-range behavior of line displacements in the direction of the driving force and in the transverse direction. We also study in detail suppression of the apparent critical force by thermal fluctuations and the temperature dependence of the trapping parameters.

The paper is organized as follows. In Section II we describe parameters characterizing the interaction between a vortex line and large-size pinning centers. In Section III we present analytical estimates. This includes formulation of general conditions for stable trapped configurations in subsection III A, making estimates for parameters of trapped line in equilibrium, subsection III B, and in the case of dynamic trapping, subsection III C. In the Section IV we describe the model used in numerical simulations. In the Section V we present our numerical results including the zero-temperature case in subsection V A and finite temperature in subsection V B In the Section VI we discuss our results and make preliminary comparisons with experiments.

II. INTERACTION BETWEEN VORTEX LINE AND PINNING CENTER

We consider first essential parameters describing interaction of vortex lines with large-size pinning centers. The vortex pinning energy by an insulating spheroid inclusion with the axes b and b_z is given by[16]

$$U_p \approx 2b_z\varepsilon_0\mathcal{L}_p, \quad \mathcal{L}_p = \ln(b/\xi_{ab}) \tag{2}$$

with $\varepsilon_0 \equiv \Phi_0^2/(4\pi\lambda_{ab})^2$.A very important parameter is the pin-breaking force, the maximum force with which the pinning center can attract the vortex line. In contrast to small defects, the pin-breaking force for large-size defects is limited by the line tension of the vortices. With increasing external force the tips of the vortex line slide along the surface of the insulating inclusion until they meet near the equator and reconnect leading to depinning of the vortex. For the in-plane current in the anisotropic layered material, the upper estimate for such line-tension-limited force can be obtained considering a simple geometry of equally-spaced pins aligned along the c-axis and neglecting interaction between vortex tips at the pin surface. In this case, evaluating the external force at which tips meet, we obtain the following estimate

$$F_p \lesssim (2\varepsilon_0/\gamma)\ln(b_z/\xi_{\min}), \tag{3}$$

where γ is the anisotropy factor and $\xi_{\min} = \max(\xi_c, s)$, ξ_c is the c-axis coherence length, and s is the interlayer period of a layered superconductor. This force only weakly depends on the size and shape of the pinning center.

Interaction of the vortex line with a remote pin is long-ranged, due to the perturbation of the supercurrent flow around the vortex by the pin,

$$U_i(r) \approx -\frac{\varepsilon_0 V_p}{\pi(1-n_y)r^2}, \text{ for } b \ll r \ll \lambda_{ab}, \tag{4}$$

where $V_p = (4\pi/3)b_z b_x^2$ is the volume of the pinning center, n_i are "depolarization factors", which depend on the parameter $\gamma b_z/b$. In particular, in the case $b_z > b/\gamma$ which includes close-to-spherical inclusions,

$$n_z = \frac{1-\zeta^2}{\zeta^3}\left(\tanh^{-1}\zeta - \zeta\right), \text{ with } \zeta = \sqrt{1-\frac{b^2}{\gamma^2 b_z^2}}$$

and $n_x = n_y = (1-n_z)/2$.

Recently, it was demonstrated that the magnetic force microscopy can be effectively used not only for imaging but also for manipulation of individual vortices[15]. This technique gives principal possibility to measure interaction between the vortex line and individual pinning center and extract relevant interaction parameters described in this section.

III. ANALYTICAL ESTIMATES FOR TRAPPING OF A VORTEX LINE

A. General condition for static pinned line

Consider a general vortex-line configuration trapped at the points $(\mathbf{u}_n, z_n)$. For simplicity, we assume that the forces from the pins are applied locally at the points $z = z_n$. In between the trapped points, $z_n < z < z_{n+1}$, the displacement obeys the following equation

$$\varepsilon_1 \frac{\partial^2 \mathbf{u}}{\partial z^2} + f\mathbf{e}_x = 0, \tag{5}$$

where f is the driving force applied along the x axis and $\varepsilon_1 = (\varepsilon_0/\gamma^2)\mathcal{L}_1$ is the line tension with $\mathcal{L}_1$ being the logarithmic factor $\mathcal{L}_1 = \ln(r_{\max}/r_{\min})$.[17] The displacement can be found as

$$\mathbf{u}(z) = \mathbf{u}_n + (\mathbf{u}_{n+1} - \mathbf{u}_n)\,\frac{z - z_n}{z_{n+1} - z_n} - \mathbf{e}_x \frac{f(z - z_n)(z - z_{n+1})}{2\varepsilon_1}. \tag{6}$$

The force acting from the pin on the vortex line at $z = z_n$ is given by

$$\mathbf{F}_n = -\varepsilon_1 \left[\frac{\partial \mathbf{u}}{\partial z}(z_n + 0) - \frac{\partial \mathbf{u}}{\partial z}(z_n - 0)\right]$$

and can be evaluated as

$$\mathbf{F}_n = -\mathbf{e}_x \frac{f(z_{n+1} - z_{n-1})}{2} - \varepsilon_1 \left(\frac{\mathbf{u}_{n+1} - \mathbf{u}_n}{z_{n+1} - z_n} - \frac{\mathbf{u}_n - \mathbf{u}_{n-1}}{z_n - z_{n-1}}\right). \tag{7}$$

The stability condition for the trapped line is given by

$$F_n < F_p \quad \text{for all } n, \tag{8}$$

while the critical state corresponds to the condition that at least one local force reaches the pin-breaking force

$$\max_n (F_n) = F_p. \tag{9}$$

One simple consequence of Eqs. (7) and (8) is that for "behind" sites, $u_{x,n} < u_{x,n-1}, u_{x,n+1}$, the line tension force adds with the external force meaning that they, in average, have shorter trapping segments $z_{n+1} - z_n$, $z_n - z_{n-1}$.

B. Equilibrium trapping

Consider trapping of a single vortex line by strong pinning centers with concentration n_p and pinning energy U_p, Eq. (2). Assuming the local equilibrium, the typical trapping length L and transverse displacement u are determined by the energy-balance condition[12]

$$\varepsilon_1 \frac{u^2}{L} = U_p,$$

and by the condition that the average number of impurities in the trapping volume should be of the order of one,

$$n_p u^2 L = 1.$$

These equations give

$$L_{\rm eq} = \sqrt{\frac{\varepsilon_1}{n_p U_p}}, \quad u^2_{\rm eq} = \sqrt{\frac{U_p}{n_p \varepsilon_1}}. \tag{10}$$

Strictly speaking, above conditions are obtained for zero current. Assuming that the trapping length does not change much when current is applied, we obtain an estimate for the critical current for the equilibrium trapping

$$\frac{\Phi_0}{c} j_{c,\rm eq} \approx \frac{F_p}{L_e} \approx F_p \sqrt{\frac{n_p U_p}{\varepsilon_1}}. \tag{11}$$

It is expected to increase with the pin density as $\sqrt{n_p}$.

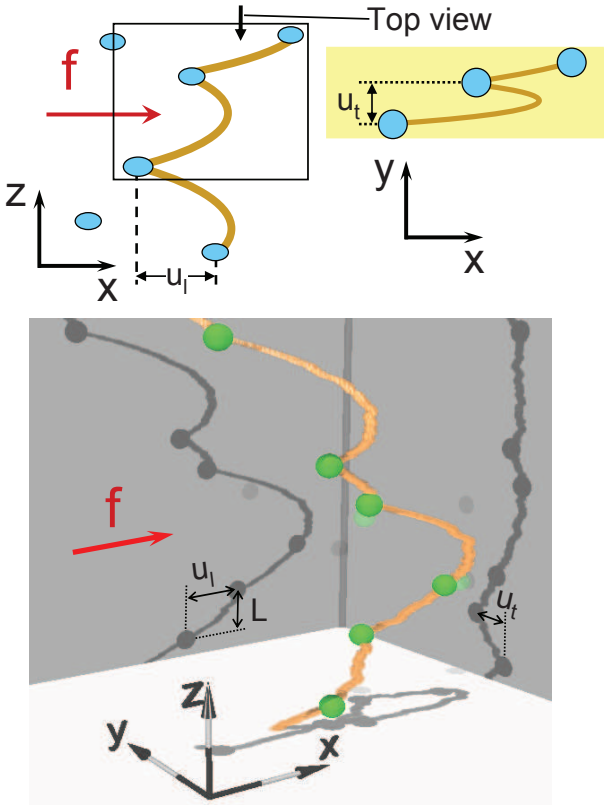

FIG. 2. *Upper figures* illustrate a trapped vortex line in the metastable regime (side and top views). The typical displacement in the direction of force u_l is much larger than the typical displacement in the perpendicular direction u_t. *Lower figure* is a visualization of the pinned line configuration obtained in simulations (only a short section of the line is shown). Shade-like projections on the axis planes illustrate line displacements in the different directions. Short scale line wiggling is due to the thermal noise. The definitions of the trapping parameters L_t, u_l, and u_t are also illustrated.

C. Dynamic trapping

The equilibrium estimates for the trapping parameters (10) are definitely valid for the line configurations prepared by cooling at fixed field and at zero transport current. However, it is clear that they can not be applied to the vortex lines in the critical state at low temperatures when moving lines are trapped after the driving force dropped below the critical value and equilibration does not take place. The critical current in such dynamic regime has been estimated in Ref. 11 for high fields when the intervortex interactions are essential. These estimates can be directly generalized to trapping of individual vortex lines at small fields.[18] When the vortex line moves close to the pinning center, it may be trapped and the line remains trapped until the force acting from the pin on the vortex line do not exceed the pin-breaking force. In this regime two typical trapping distances, in the direction of motion, u_l, and in the transverse direc-

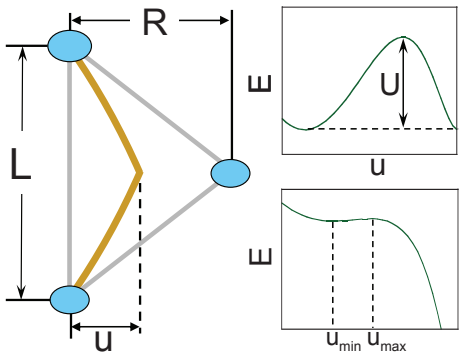

FIG. 3. Trapped segment interacting with pinning center. The upper right plot illustrates the energy profile for the value of R below which the trapping becomes energetically favorable but separated by the energy barrier. The lower right plot illustrates the energy profile near the trapping instability point.

tion, u_t, are very different and have very different origins, see Fig. 2. These distances and the trapped-segment length L are connected by the geometrical relation

$$n_p L u_l u_t = 1. \tag{12}$$

The longitudinal trapping distance, u_l, is determined by the pin-breaking condition,

$$\varepsilon_1 \frac{u_l}{L} = F_p. \tag{13}$$

This condition can be obtained from x component of Eq. (7) assuming that the two terms in the right hand side are of the order of the pin-breaking force.

The transverse displacement between the pins u_t is determined by the trapping events. The simplest assumption is that in most cases trapping occurs when the lines directly collide with the pins[18] meaning that $u_t \approx b$. This immediately gives estimates for other trapping parameters,

$$u_l = \sqrt{\frac{F_p}{n_p \varepsilon_1 b}},\ L = \sqrt{\frac{\varepsilon_1}{n_p b F_p}}. \tag{14}$$

This corresponds to the following result for the critical current

$$\frac{\Phi_0}{c} j_{c,\mathrm{tr}} = F_p^{3/2} \sqrt{\frac{n_p b}{\varepsilon_1}}. \tag{15}$$

Note that in this situation the estimate is somewhat similar to the equilibrium case, Eq. (11), and has the same dependence on the pin density, $\propto \sqrt{n_p}$. The physical assumptions behind the two estimates, however, are completely different.

The above simple assumption, however, may underestimate u_t. Due to the long-range pin-vortex interaction (4) a pinning center may capture the vortex line even without direct collisions. When the line passes sufficiently close to the pinning center it may be trapped by this center due to instability. To estimate the maximum transverse trapping distance u_t, we consider interaction energy of the segment of length L with pinning center located at distance $R \gg b$,[11] see Fig. 3,

$$E(u) = \varepsilon_1 \frac{2u^2}{L} - \frac{A\varepsilon_0 V_p}{(R-u)^2}.$$

with $A = 1/[\pi(1-n_y)]$. This gives the interaction force

$$F(u) = \varepsilon_1 \frac{4u}{L} - \frac{2A\varepsilon_0 V_p}{(R-u)^3}$$

Introducing the reduced variables

$$x = \frac{u}{R},\ W = \frac{A\varepsilon_0 L V_p}{2\varepsilon_1 R^4},$$

we rewrite the energy and force as

$$E = \varepsilon_1 \frac{2R^2}{L}\left[x^2 - \frac{W}{(1-x)^2}\right],$$
$$F(x) = -\varepsilon_1 \frac{4R}{L}\left(x - \frac{W}{(1-x)^3}\right).$$

The equilibrium points are determined by

$$x(1-x)^3 = W.$$

The instability point corresponds to the value of W when the equilibrium points vanish which happens at $W > W_{\max} = \max[x(1-x)^3] = 3^3/4^4$. Therefore the condition for the instability can be written as

$$\frac{A\varepsilon_0 L V_p}{2\varepsilon_1 u_t^4} = \frac{3^3}{4^4},$$

which determines the maximum trapping distance u_t as

$$u_t = 4\left(\frac{A\varepsilon_0 L V_p}{54\varepsilon_1}\right)^{1/4}. \tag{16}$$

The vortex line will be trapped by the pinning centers located closer than this distance in the direction perpendicular to the driving force. Note that the numerical coefficient in this equation should not be taken too literally because it is only correct for the simplest geometry illustrated in Fig. 3. Using this result, we find from Eqs. (12) and (13)

$$L_{\mathrm{tr}} = \left[\frac{\varepsilon_1^{5/4}}{n_p F_p \left(\varepsilon_0 V_p\right)^{1/4}}\right]^{4/9}, \tag{17}$$

$$u_l = \left[\frac{F_p^{5/4}}{n_p \varepsilon_1 \left(\varepsilon_0 V_p\right)^{1/4}}\right]^{4/9}, \tag{18}$$

$$u_t = \left[\frac{\varepsilon_0^2 V_p^2}{n_p \varepsilon_1 F_p}\right]^{1/9}. \tag{19}$$

This gives the following estimate for the critical current

$$\frac{\Phi_0}{c} j_{c,\mathrm{tr}} = \frac{n_p^{4/9} F_p^{13/9} (\varepsilon_0 V_p)^{1/9}}{\varepsilon_1^{5/9}} \tag{20}$$

Comparing this result with the critical current for the equilibrium regime (11), we can see that two regimes are characterized by somewhat different dependence on parameters. However, dependences on the pin density occur to be close, the exponent in the power low, $j_c \propto n_p^{\alpha}$ in this dynamic-trapping regime is somewhat smaller than the power 1/2 for the equilibrium regime, $\alpha = 4/9 \approx 0.444$.

D. Typical pin-breaking force at finite temperatures

At finite temperature the line is moving at all driving forces but at small forces the very slow motion occurs due to the rare thermally activated jumps (creep regime). The creep and flow regimes are separated by the effective critical force which can be evaluated using a velocity criterion. Such defined the effective critical force is temperature dependent and thus differs from the sharply defined zero-temperature critical force of the depinning transition, but it has the advantage that it can be directly compared with experimental estimates. We do not consider creep in this paper and our purpose is to evaluate suppression of this critical force by the thermal noise. The main mechanism of thermal suppression is reduction of the effective pin-breaking force. At finite temperature the trapped vortex segment has a finite life time on the pin even if the pinning force F is smaller than the maximum pin-breaking force. To quantify this effect, we can introduce the temperature-dependent force $\tilde{F}_p(T) < F_p$ at which the trapped segments is typically released from pins.

To evaluate this force, we assume that the line motion in the crossover region consists of segment jumps, meaning that the average line velocity can be estimated as $v \approx u_l/\tau$, where $\tau = \tau_0 \exp[U(F)/T]$ is the typical time during which the vortex segment remains pinned and $U(F)$ is the typical energy barrier for detrapping. When the force F acting from the pin is only slightly smaller than the maximum pin-breaking force, the barrier behaves as in the single-particle case,[19] $U(F) = a_F U_p (1 - F/F_p)^{3/2}$, where $a_F = 4\sqrt{2} F_p^{3/2}/(3U_p\sqrt{|F_p''|})$ and F_p'' is the second derivative of the interaction force with respect to the line displacement at the maximum-force point. The velocity criterion for the effective critical force can be written as $\eta v = C_f f_c$ where η is the viscosity coefficient and $C_f \ll 1$. At small temperatures this gives us the following relation for $\tilde{F}_p$

$$\frac{\tau_0}{\eta} \exp\left[\frac{a_F U_p}{T}\left(1 - \frac{\tilde{F}_p}{F_p}\right)^{3/2}\right] \approx \frac{u_l}{C_f f_c}.$$

Using the estimate $f_c \approx \tilde{F}_p/L_t$, geometrical relation (12) and assuming for simplicity that $u_t \approx b$, we obtain

$$\tilde{F}_p(T) \approx F_p \left[1 - \left(\frac{T}{a_F U_p} \ln \frac{\eta}{C_f \tau_0 \tilde{F}_p n_p b}\right)^{2/3}\right]. \tag{21}$$

We expect that at small temperatures the effective critical force and trapping parameters can be roughly evaluated using simple replacement $F_p \to \tilde{F}_p(T)$.

IV. MODEL FOR NUMERICAL SIMULATIONS

To develop quantitative understanding of the strong pinning by the array of inclusions, we numerically simulated motion of the vortex line described by the dynamic equation

$$\eta \frac{\partial \mathbf{u}}{\partial t} = \varepsilon_1 \frac{\partial^2 \mathbf{u}}{\partial z^2} + \sum_j \mathbf{F}(\mathbf{u} - \mathbf{R}_j)\delta(z - z_j) + \mathbf{e}_x f + \mathbf{F}_T(z,t). \tag{22}$$

Here f is the driving force along x direction from the current, $(\mathbf{R}_j, z_j)$ are the random pin coordinates, $\mathbf{F}_T(z,t)$ is the Langevin thermal force

$$\langle F_{T,\alpha}(z,t) F_{T,\alpha'}(z',t')\rangle = 2\eta T \delta_{\alpha\alpha'}\delta(t-t')\delta(z-z'),$$

and

$$\mathbf{F}(\mathbf{u}) = -\frac{\partial U(\mathbf{u})}{\partial \mathbf{u}}$$

is the interacting force with a strong pin. We model the interaction potential by the function

$$U(\mathbf{u}) = -\frac{U_p b^2 G_{\mathrm{cut}}(u)}{u^2 + b^2}, \tag{23}$$

where the cutoff function $G_{\mathrm{cut}}(u)$ is introduced for numerical convenience, $G_{\mathrm{cut}}(u) = (1 - u^2/R_{\mathrm{cut}}^2)^2$ for $u < R_{\mathrm{cut}}$ and $G_{\mathrm{cut}}(u) = 0$ for $u > R_{\mathrm{cut}}$ with $R_{\mathrm{cut}} \gg b$. An important feature which never was taken into account in modeling is the long $1/u^2$ tail in the interaction potential. However, this model does not describe the line-tension limited pin-breaking force. In our model the pin-breaking force from an isolated pin is given by $F_p = (3\sqrt{3}/8)U_p/b$ which is achieved at $u = b/\sqrt{3}$. The model in its original form has an unrealistic feature. For improbable configurations when many pins are located at distances smaller than b, the vortex interaction with such a cluster may increase without limit. This, of course, does not happen in real superconductors. To bring our model somewhat closer to reality, we renormalized the total pin-vortex interaction force as $\mathbf{F}_{\mathrm{v-p}}(\mathbf{u}) = \sum_j \mathbf{F}(\mathbf{u} - \mathbf{R}_j)$ as

$$\mathbf{F}_{\mathrm{v-p}} \to \mathbf{F}_{\mathrm{v-p}} \frac{\tanh(F_{\mathrm{v-p}}/F_{\mathrm{lim}})}{F_{\mathrm{v-p}}/F_{\mathrm{lim}}},$$

so that the maximum force can not exceed $F_{\rm lim}$. This modification has only minor influence on the interaction of the vortex line with an isolated pin.

For numerical implementation of the model, we use the reduced variables

$$\mathbf{u} = b\tilde{\mathbf{u}},\ z = \frac{\varepsilon_1 b^2}{U_p}\tilde{z},\ t = \frac{\eta\varepsilon_1 b^4}{U_p^2}\tilde{t},$$
$$\mathbf{f} = \frac{U_p^2}{\varepsilon_1 b^3}\tilde{\mathbf{f}},\ \tilde{\mathbf{F}}(\tilde{\mathbf{u}}) = \frac{\partial}{\partial\tilde{\mathbf{u}}}\frac{G_{\rm cut}(\tilde{u})}{\tilde{u}^2+1},$$

in which the equation takes the simpler form

$$\frac{\partial\tilde{\mathbf{u}}}{\partial\tilde{t}} = \frac{\partial^2\tilde{\mathbf{u}}}{\partial\tilde{z}^2} + \sum_j \tilde{\mathbf{F}}(\tilde{\mathbf{u}}-\tilde{\mathbf{R}}_j)\delta(\tilde{z}-\tilde{z}_j) + \mathbf{e}_x\tilde{f} + \tilde{\mathbf{F}}_T(z,t) \quad (24)$$

with

$$\left\langle \tilde{F}_{T,\alpha}(\tilde{z},\tilde{t})\tilde{F}_{T,\alpha'}(\tilde{z}',\tilde{t}')\right\rangle = 2\tilde{T}\delta_{\alpha\alpha'}\delta(\tilde{t}-\tilde{t}')\delta(\tilde{z}-\tilde{z}')$$
$$\tilde{T} = T/U_p$$

In this dimensionless form, the equation depends only on the reduced temperature and reduced pin density $\tilde{n}_p = (\varepsilon_1 b^4/U_p)n_p$. The condition of strong pinning regime is $n_p < U_p/\varepsilon_1 b^4$ corresponding to $\tilde{n}_p < 1$. For typical parameters $\gamma = 5$, $b_z = b = 10$nm, and $n_p = (100\text{nm})^{-3} = 10^{15}\text{cm}^{-3}$, the reduced pin density can be estimated as $\tilde{n}_p \approx n_p b^4/(b_z\gamma^2) \approx 10^{-4}$. In simulations we mostly used $\tilde{F}_{\rm lim} = 1$. For an isolated pin this gives the pin-breaking force $\tilde{F}_p = \tanh(3\sqrt{3}/8) \approx 0.57$. We also used $\tilde{R}_{\rm cut} = 50$ in the cutoff function $G_{\rm cut}(\tilde{u})$. We consider systems of size $L_x \times L_y \times L_z$, where L_z is the vortex-line length, L_x is the size in the direction of displacements and L_y the size in the transverse direction.

One of our tasks is to compute the dependence of the critical force on the density of pinning centers. The calculation of the steady-state critical force is not as trivial problem as it may look. For a finite-size system there is always a metastable configuration giving the maximum depinning force. Assuming that such configuration is always reachable from any initial condition at long times this would be the critical force we seek. In a large system this configuration is however determined by rare nontypical configuration of pins. As a consequence, the maximum depinning force slowly grows with the increasing the system sizes L_x and L_y, meaning that it is not a self-averaging parameter for a fixed line length L_z. To avoid this a carefully chosen (anisotropic) thermodynamic limit in all directions was proposed for $d+1$ dimensions[25]. The maximum depinning force of the very large system is also very difficult to compute. Simulations of Eq. (24) at zero temperature are not very suitable for this purpose, because when the external force is close to critical value, the vortex line traps forever in the first metastable state it finds and it is not clear how representative is this state and how close the corresponding critical force to the maximum value. In addition, neither the maximum critical force nor depinning forces for few accidental metastable states are very interesting quantities from the practical point of view. The maximum critical force is essentially property of an isolated vortex line. A more interesting quantity is the typical pinning force for the finite density of the vortex lines. Indeed, even at low densities when vortex-vortex interactions can be neglected, we expect a typical pinning force rather than an extreme non-self averaging force value determines the observable critical current.

To evaluate a typical pinning force at zero temperature, instead of fixed-force approach, we employ the fixed-velocity simulations using approach suggested in Ref. 20. Namely, we replaced the fixed external force $\tilde{f}$ in Eq. (24) with slowly moving parabolic potential,

$$f \to K\left[W(t) - u_x(z,t)\right],\ W(t) = W_0 + Vt \quad (25)$$

Such potential forces the vortex line to move with the average velocity V. Every time the line finds a metastable pinned state and stops, the dragging force starts to increase with time until it exceeds the critical force for this state and line will resume motion. This trick allows us to explore many metastable states and to avoid the extreme value statistics of the sample-dependent critical force. The typical critical force is then evaluated as the average force acting on the vortex line in the critical configurations,

$$f_c = \langle\langle K\left[W(t) - u_x(z,t)\right]\rangle_z\rangle_t \quad (26)$$

where $\langle\ldots\rangle_t$ implies averaging over the local maxima of the instantaneous force. The spring constant K and the drag velocity V have to be taken sufficiently small so that they do not influence calculation of the critical force. We typically use $K \sim 10^{-5} - 10^{-6}$ and $V = 0.001 - 0.002$. The spring constants satisfy $K \sim L_z^{-2}$ in each case, assuring a proper thermodynamic limit for the critical force and associated critical configuration[20], and the velocities are small enough to assure a quasistatic stick-slip motion. Figure 4(left) illustrates the typical dependences of the force acting on the line on the displacement of its center of mass for different pin densities n_p and line lengths N_z.

We also explore the velocity-force dependences at finite temperatures using the direct fixed-force simulations described by Eq. (24). Even though the term "critical force" is widely used in the experimental community, at finite temperatures the concept of the critical force does not have exact meaning because the velocity is finite at all forces due to the thermal creep. Nevertheless, one can still introduce the characteristic force describing crossover between the flux-flow and flux-creep regimes using some average-velocity criterion. At low temperatures near such critical force the line motion becomes very uneven, see Fig. 4(right). It spends considerable time in metastable traps waiting for a strong fluctuation which would allow it to continue the motion. Such line motion is illustrated by animation[21]. As a consequence, a proper averaging over such events requires huge simulation times and/or averaging over many realization of the

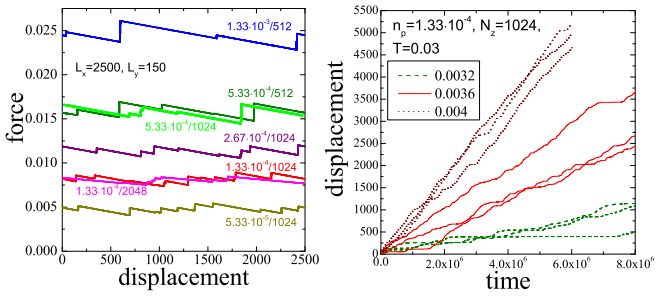

FIG. 4. *Left:* Representative dependences of the force acting on the line versus its center of mass location obtained using the fixed-velocity simulations for different pin densities n_p and line lengths N_z (the curves are marked by n_p/N_z). The vertical segments correspond to trapped states. The typical critical forces, f_c, are obtained by averaging of over local maxima of these curves. *Right:* Examples of the displacement-time dependences used to evaluate average velocities at fixed temperature for the parameters shown in the plot and for different forces. Each force is represented by three curves corresponding to different realizations of the random potential. The line motion becomes more and more uneven with decreasing force.

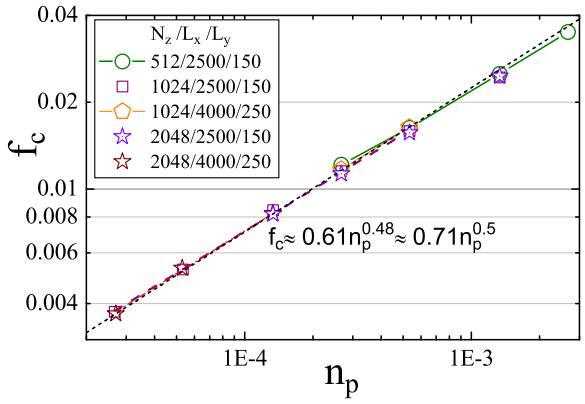

FIG. 5. The dependence of the critical force on the pin density. The plot contains data obtained for different system sizes, the legend shows $N_z/L_x/L_y$. The finite-size effects in the critical force are weak.

random potential. In addition to the critical force, we explore statistical parameters of trapping which allow us to understand better the pinning mechanism. We evaluated the average length of trapped segment L_t, typical displacements along the motion direction u_l and in the perpendicular direction u_t. We studied the distribution of these parameters and their evolution with temperature and force. We also studied the long-range wandering of the line in the direction of motion and in the transverse direction.

For numerical solution the reduced equation (24) has to be discretized both in time and in z-coordinate. We typically used $dt = 0.05 - 0.1$ and $dz = 1$ for the discretization steps. To study finite-size effects, the equation was solved for the different numbers of slices in z directions, $N_z \equiv L_z/dz$, ranging from 512 to 2048.

V. NUMERICAL RESULTS

A. Behavior at zero temperature

We systematically studied behavior of the critical force and properties of trapped line configurations within the pin density range spanning two orders of magnitude, from $2.7\cdot10^{-5}$ to $2.7\cdot10^{-3}$. Figure 5 presents the dependences of the critical force f_c on the pin density n_p for different systems sizes N_z. We found that f_c increases with n_p according to the power law $f_c = f_0 n_p^\alpha$. The fit gives for the power index the value slightly smaller than $1/2$, $\alpha \approx 0.48$ and the coefficient $f_0 \approx 0.61$. In fact, a square-root dependence $f_c \approx 0.71\sqrt{n_p}$ also provides reasonable description of the data. The power is, however, clearly larger than the value 0.44 suggested by the dynamic-trapping

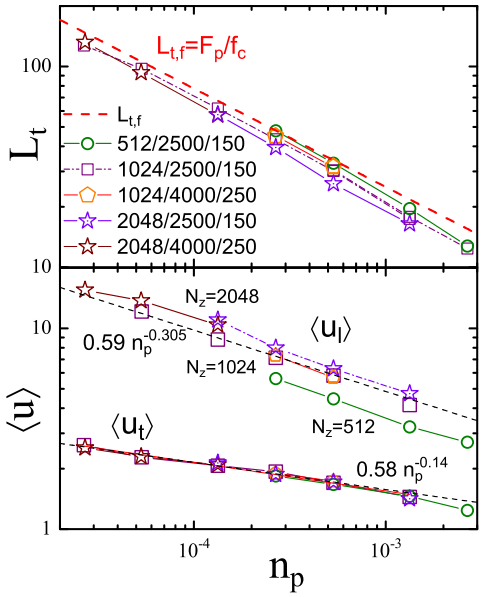

FIG. 6. Summary of pin-density dependences of trapping parameters for different system sizes. As in the previous plot, the legend shows $N_z/L_x/L_y$. *Upper plot:* The dependences of the average trapped-segment length L_t. For comparison, we show the expected trapping length extracted from the critical force. *Lower plots:* The pin-density dependences of the average pin-to-pin displacements in the directions of the force (longitudinal) and in the perpendicular direction (transverse). The longitudinal displacement, $\langle u_l \rangle$, has considerable finite-size effect with respect to the line length N_z.

estimates in the case when trapping occurs due to instabilities. For the used line lengths $N_z \geq 512$ a noticeable finite-size effect becomes visible only for small pin densities $n_p < 3\cdot10^{-4}$.

To understand statistical properties of trapped configuration, we plot in Fig. 6 the pin density dependences

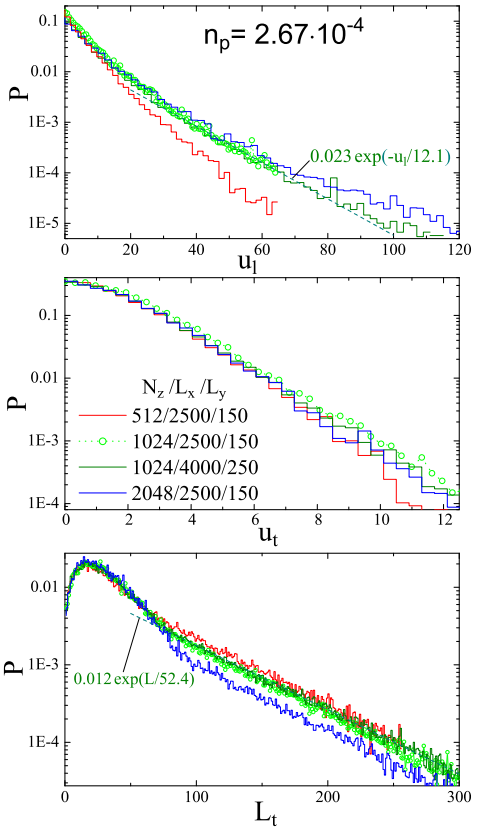

FIG. 7. Examples of distribution functions of trapping parameters at one pin density and for different system sizes.

of the average trapping parameters defined in Fig. 2, the trapping length L_t, the pin-to-pin displacements along the direction of force u_l and in the transverse direction u_t. In the plot $L_t(n_p)$ we show the expected value of the typical trapped segment extracted from the value of the critical force $L_{t,f} = F_p/f_c$. We can see that the real trapping segments extracted from the configurations are indeed follow closely the expected values. We also see that the average trapping segments are systematically smaller that the segments which determine the critical force. This a natural behavior because one can expect that the critical force is determined by "weak spots" where the trapping segments are longer than average along the line. The difference, however, is not very significant. The trapping length shows a weak but unexpected size effect, it slightly *decreases* with the increasing total line length. We found that the product $n_p L_t u_l u_t$ which on general ground is expected to be of the order unity is, in fact, slowly decreases with n_p from ~ 0.18 to ~ 0.14.

From the plots of the pin-to-pin displacements we can see that the pinned configurations are strongly anisotropic, the average displacement along the direction of the driving force u_l significantly exceeds the displacement in the transverse direction u_t. This is consistent with the dynamic-trapping picture described in Sec. III C. The difference grows with decreasing pin density n_p. In addition, the longitudinal displacement shows a significant size effect, it grows with increasing system size N_z. Further analysis shows that this is an indication of growing local stresses with increasing line length and suggests destruction of the vortex lines by the pinning potential in the critical state for the sufficiently large systems. This behavior is not anticipated by the simple estimates. It is interesting to note, however, that this size effect in u_l does not lead to the significant size dependence of the critical force. On the other hand, the average transverse displacement u_t does not show any size effect. It slowly grows with decreasing n_p from 1.24 at $n_p = 0.0027$ to 2.54 at $n_p = 2.7 \cdot 10^{-5}$. As u_t remains comparable with the defect size, the regime in which the transverse trapping is determined by the long $1/r^2$ tail of pin-vortex interaction is not quite realized. This explains why the power index in the force-pin density dependence is larger than suggested by the metastable-regime estimates which assume $u_t \gg 1$. To obtain further insight on properties of trapped lines we show in Fig. 7 examples of the distribution functions of trapping parameters for fixed density $n_p = 2.67 \cdot 10^{-4}$ and different system sizes. One can see that these distributions are characterized by the long exponential tails. There is a noticeable probability to find segments with very large u_l and L_t. Note that the tails have opposite size effects for these parameters, probability to find large u_l increases with N_z while probability to find large L_t *decreases* with N_z. The last trend is opposite to naive expectations.

To characterize the long-range displacements of the line, we studied behavior of the structure factors, the Fourier transforms of the displacement correlation functions,

$$S_{l,t}(q) = \frac{1}{N_z} \left\langle \left| \sum_{z=1}^{N_z} u_{x,y}(z) \exp(-iqz) \right|^2 \right\rangle . \qquad (27)$$

The examples of these quantities are presented in Fig. 8 (left) for two pin densities. Similar to local quantities, the long-range displacements are also strongly anisotropic. Such anisotropic scaling of displacements is a general property of the driven lines in the critical regime independent of pinning mechanism.[22] For both components we clearly observe two regions of q characterized by different power-law dependences $S_{l,t} \propto q^{1+2\zeta_{l,t}}$. For smallest q's we found the roughness exponents $\zeta_l \approx 1.14$ and $\zeta_l \approx 0.45$. The value of $\zeta_t < 1$ for the transverse direction corresponds to the line displacements increasing as $\langle [u_y(z) - u_y(0)]^2 \rangle \propto z^{2\zeta_t}$ at large z. On the other hand, the found value of $\zeta_l > 1$ for the longitudinal displacements implies that the assumed elastic approximation is not self-consistent in the thermodynamic limit, the average local stress $\langle (du_x/dz)^2 \rangle$ increases with the line length L_z as $L_z^{2(\zeta_l - 1)}$. In this case the longitudinal line displacements grow quadratically $\langle [u_y(z) - u_y(0)]^2 \rangle = C_l z^2$ with the coefficient increasing with the line length as

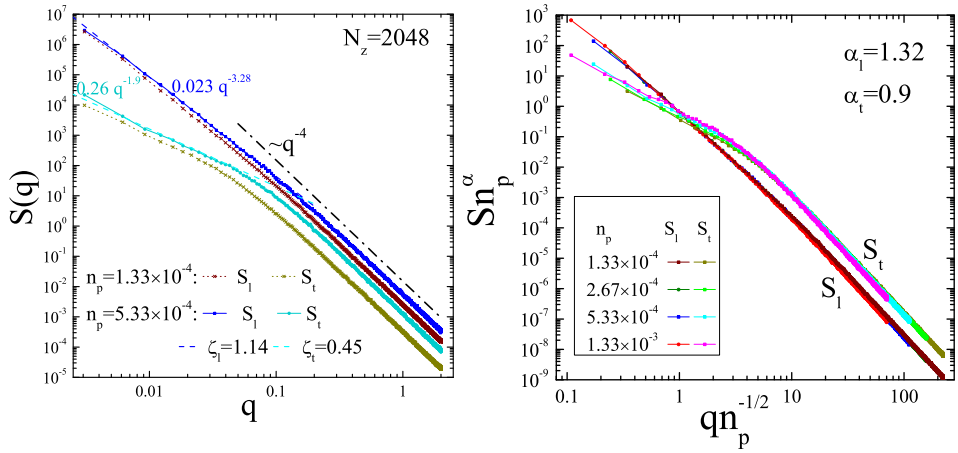

FIG. 8. *Left:* Transverse and longitudinal structure factors of the line for $N_z = 2048$ and two densities of pins. Two regions of power-law q-dependences for both components are clearly observed for both components. *Right:* Scaled structure factors for different pin densities.

$C_l \propto L_z^{2(\zeta_l-1)}$.[23] This provides a natural explanation for the strong size dependence of the longitudinal pin-to-pin displacement u_l in the lower plot of Fig. 6. The negative size effects for the trapping lengths in the upper plot of the same figure also can be understood. Growing local stress with increasing N_z forces the line to travel longer distances in the longitudinal direction which increases the probability to find a pin separated by smaller distance in z direction.

The found exponents are slightly different from the values $\zeta_l = 1$, $\zeta_t = 0.5$ obtained in Ref. 22 from the approximate functional renormalization group calculations. However, a similar situation was found for elastic lines in a plane where numerically computed index $\zeta = 1.25$[24,26] also exceed the predicted value $\zeta = 1$. We see that the transverse displacements somewhat reduce the exponent value in the 3D case. Since the small-q exponents are expected to be universal, i.e., independent of the pinning mechanism, our results suggest that the elastic description will break down also for the weak pinning case. Although we have considered the linear approximation for the elastic forces, this conclusion is expected to hold for the full non-quadratic energy of the deformed vortex line.[24]

At larger q's we observe the regime where both components behave as $S_{l,t} = A_{t,l}q^{-4}$ giving the short-scale indices $\zeta_l = \zeta_t = 3/2$. This corresponds to displacements induced by a short-correlated random force and such behavior is actually similar to the static Larkin regime for weak pinning. However, the random forces in our case clearly has very different origin.

The crossover between different regimes occurs at the wave vector which scales approximately as $\sqrt{n_p}$. This allows us to approximately collapse the structure factors at different pin densities into a single curve using scaling $S_{l,t}(q) = n_p^{-\alpha_{l,t}} G_{l,t}(q n_p^{-1/2})$. We found $\alpha_l \approx 1.32$ and $\alpha_t \approx 0.9$. These scaled dependencies are shown in the right part of Fig. 8. Scaling works better for the longitudinal structure factor. This scaling is consistent with the identification of the trapping parameter $L_t(n_p)$ as a geometrical crossover length at $qL_t \sim 1$, between a short distance roughness regime with exponents $\zeta_l = \zeta_t = 3/2$ and the large distance universal regime with exponents $\zeta_t \approx 0.45$ and $\zeta_l \approx 1.14$. This behavior is again very similar to the crossover between the Larkin regime and the random-manifold regime established for the case of weak collective pinning even though disorder is not weak in the present case.

We can also see from Fig. 8(left) that the both structure factors increase with the pin density for all wave vectors. This means that, in contrast to elemental pin-to-pin displacements $u_{l,t}$ plotted in Fig. 6, the line displacements at fixed z *grow* with increasing pin density. This behavior can be easily understood. The displacements at small distances are determined not only by behavior of $u_{l,t}$ but also by behavior of the trapping length L_t. All these parameters decrease with increasing pin density, meaning that smaller displacements occur at smaller length scale. The net increase of the line displacements at fixed z coordinate with increasing n_p is a consequence of faster $L_t(n_p)$ decrease than $u_{l,t}(n_p)$, as it can be seen from Fig. 6.

B. Dynamics at finite temperatures

In this section we consider influence of thermal noise on dynamic response and configurations of vortex lines interacting with strong pins. Figure 9 presents the temperature evolution of the velocity-force dependences and trapping parameters in the critical region for two very different pin densities, $n_p = 5.33 \times 10^{-5}$ and $n_p = 1.33 \times 10^{-3}$. We remind that we use the pinning energy of single pin as the temperature units. At finite temperature the crit-

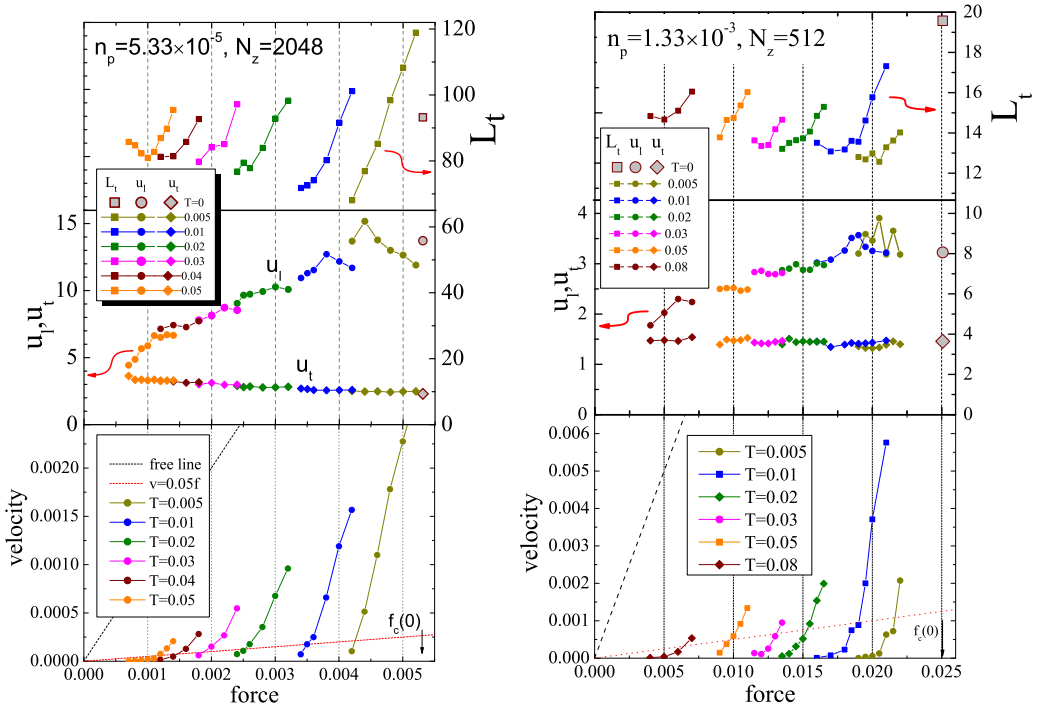

FIG. 9. The temperature evolution of the velocity-force dependences (bottom plots), lengths of trapped segments (top plots, right axes), and pin-to-pin displacements (middle plots) for two very different pin densities, $n_p = 5.33 \times 10^{-5}$ (left) and 1.33×10^{-3} (right) in the regions corresponding to crossover between flow and creep.

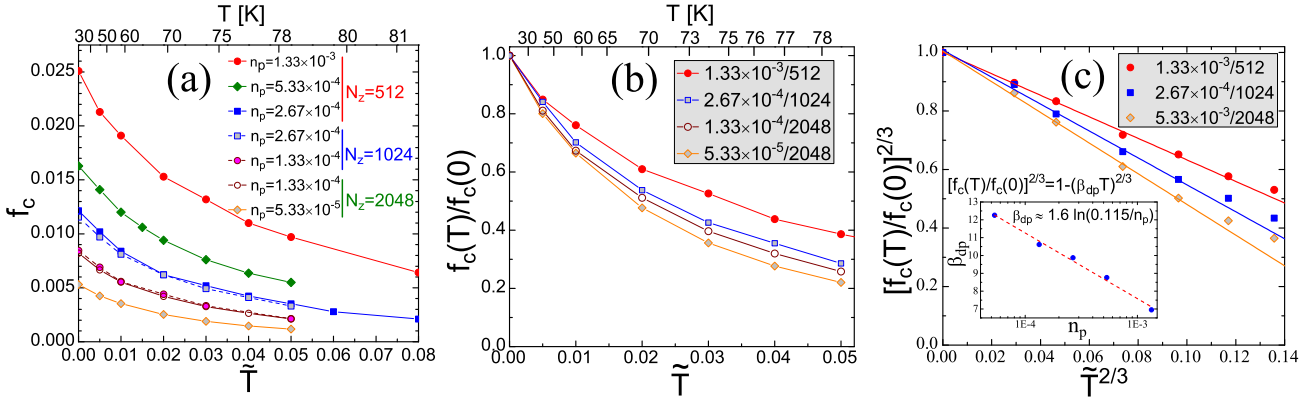

FIG. 10. (a) Temperature dependences of the effective critical forces for different pin densities and line lengths. (b) Relative suppression of effective critical forces by thermal fluctuations for selected pin densities/line lengths. (c) Plots of $[f_c(T)/f_c(0)]^{2/3}$ vs $T^{2/3}$ showing approximately linear dependences in agreement with Eq. (21). The inset shows the pin-density dependence of the coefficient β_{dp} with the logarithmic fit. Legends in the plots (b) and (c) imply n_p/N_z. The top axes in the plots (a) and (b) provide the approximate real temperature scales computed for spherical particles with radius $b = 5$ nm assuming $\lambda_{ab} = 140nm/\sqrt{1-(T/T_c)^2}$ with $T_c = 90$ K.

ical force does not have exact meaning, because the line velocity is finite at all forces due to the thermal creep. Nevertheless, we can introduce the typical force corresponding to the crossover between the flow and creep regimes, similar to voltage criterion widely used in experiment. We use the criterion $v = 0.05f$ for this force. The first important observation is that, independently of criterion, the apparent critical force is quite strongly suppressed by the thermal noise. For example, as we can see in Fig. 9, for small pin density $n_p = 5.33 \times 10^{-5}$ at temperature only 5% of the pinning energy, the apparent critical force is already suppressed about four times.

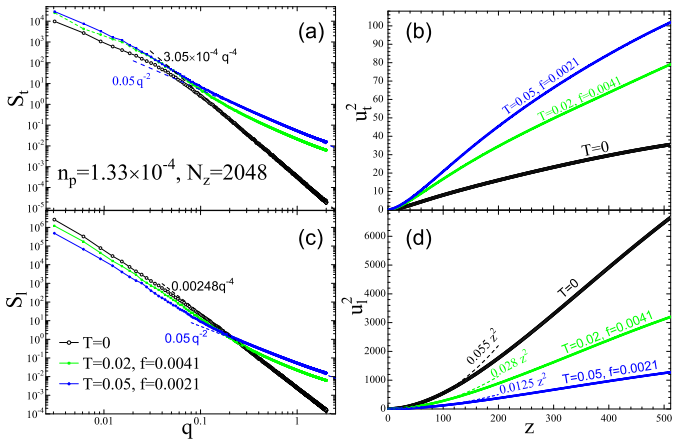

FIG. 11. Typical evolution of the structure factors (plots (a) and (c)) and line displacements (plots (b) and (d)) with increasing temperature for one pin density. Thermal fluctuations in the critical regime reduce the line displacements in the direction of drive and increase the line displacements in the transverse direction.

As one can see from the trapping parameters plots, the longitudinal pin-to-pin displacement u_l in the critical region very rapidly decreases with the temperature while the transversal displacement u_t slightly increases with the temperature. As a consequence, at some temperature they become of the same order. The longitudinal displacement typically has nonmonotonic dependence on the driving force and reaches maximum at some force in the critical region (the maximum-stress force). The trapping length decreases with decreasing line velocity and its value at $v = 0.05f$ slightly increases with the temperature.

Figure 10(a) shows the temperatures dependences of the apparent critical forces for a wide range of pin densities. We can see that these dependences are quite similar. However, plots of the relative critical forces in Fig. 10(b) clearly show that thermal suppression weakens with increasing pin density. This is consistent with the estimate for the temperature renormalization of the effective pin-breaking force, Eq. (21), due to the n_p dependence under the logarithm. For illustration, we also present the real-temperature scales on the top axes of plots in Fig. 10(a,b) computed for spherical particles with $b = 5$nm and typical YBCO parameters. This scale, however, is very sensitive to the value of b. For example, the liquid nitrogen temperature $T = 77$K corresponds to the reduced temperature $\tilde{T} \approx 0.041$ in the plot. For particles with $b = 10$nm the same real temperature would correspond to much smaller value $\tilde{T} \approx 0.011$.

As we found approximately $f_c \propto \sqrt{n_p}$ at $T = 0$, according to estimate (15) we also expect the relation $f_c \propto F_p^{3/2}$. This means that, according to Eq. (21), we expect the dependence $[f_c(\tilde{T})/f_c(0)]^{2/3} = 1 - (\beta_{dp}\tilde{T})^{2/3}$ with $\beta_{dp} = (1/a_F)\ln(n_{p0}/n_p)$. This is directly verified in Fig. 10(c) where we observe the approximate linear dependencies of $[f_c(\tilde{T})/f_c(0)]^{2/3}$ versus $\tilde{T}^{2/3}$. Moreover, as shown in the inset, the coefficient β_{dp} found from the linear fits for different pin densities indeed has logarithmic dependence on n_p, $\beta_{dp} \approx 1.6\ln(0.115/n_p)$. These observations provide justification to our assumption that reduction of the typical pin-breaking force is the main source of thermal suppression of the effective critical force.

We consider now the influence of thermal noise on the long-range behavior of the line displacements. Figure 11(a,c) presents evolution of the structure factor with increasing temperature for pin density $n_p = 1.33 \times 10^{-4}$. We can see that the slope of the small-q dependences does not change indicating that the roughening indices ζ_l and ζ_t are temperature independent. However, the coefficient is significantly reduced for the longitudinal displacements and is enlarged for the transverse displacements. Correspondingly, as one can see from the line wandering plots shown in Fig. 11(b,d), the components of displacements in the critical region have opposite tendencies: the longitudinal displacements decrease and and the transverse displacement increase with increasing temperature. As the longitudinal displacements dominate, the lines become more straight in the critical region. Another important observation is that the random-force regime $S_{l,t} \propto q^{-4}$ at large q is rapidly washed out by thermal noise for both components and is replaced by the isotropic fluctuational line wandering $S_{l,t} = T/q^2$.

VI. DISCUSSION AND COMPARISON WITH EXPERIMENT

Using the square root fit of the pin-density dependence of critical force in Fig. 5, we can restore n_p-dependence of the critical force in real units

$$f_c = 1.9F_p^{3/2}\sqrt{\frac{n_p b}{\varepsilon_1}} \tag{28}$$

This coincides with estimate (15) which is obtained assuming that the transverse trapping distance u_t is of the order of pin size b. This does not contradict too much our numerical results, because our average values of u_t only slightly exceed the pin size. Note that in our simulations the pin-breaking force F_p is fixed by interaction with the pin while in real superconductors for large-size inclusions it is determined by the in-plane line energy, see Eq. (3). Substituting this estimate, our result leads to the following estimate for the critical force

$$f_c = A_c\varepsilon_0\sqrt{n_p b/\gamma},$$

where, assuming $\xi_c < s$, we estimated $A_c \lesssim 5.4[\ln(b_z/s)]^{3/2}[\ln(L_t/s)]^{-1/2}$.

For preliminary comparison with experiment we use results of the recent paper 7 in which approximately spher-

ical $(Y\text{-}Gd)_2O_3$ particles with radius ~ 4 nm were embedded into the YBCO films. The typical concentration of particles was $5 \times 10^{16}\text{cm}^{-3}$. For estimates, we assume the temperature-dependent London penetration depth as $\lambda_{ab} = 140\text{nm}/\sqrt{1-(T/T_c)^2}$ with $T_c = 90\text{K}$ and the anisotropy $\gamma = 5$. Such parameters correspond to the reduced concentration $\tilde{n}_p \approx 1.3 \times 10^{-4}$. From the above zero-temperature result, we estimate $A_c \approx 3.9$ and the critical current $j_c \approx 1.7 \times 10^7$ amp/cm^2 which is close to the low-field experimental value at 5K, 2.08×10^7 amp/cm^2. The reduced temperature can be evaluated as $\tilde{T} \approx (T/5.3 \times 10^3 K)/(1-(T/T_c)^2)$. At 55K this gives $\tilde{T} \approx 0.017$. According to Fig. 10(b), at this temperature thermal suppression of the critical current is expected to be around 50%. Taking this factor and the temperature dependence of parameters into account, we expect critical current $j_c \approx 5.2 \times 10^6$ amp/cm^2, which again is quite close to the experimental value 6.22×10^6 amp/cm^2. We can conclude that the our strong-pinning result for the critical current is in reasonable agreement with experiment.

Our results show that the wandering of dynamically pinned lines is strongly anisotropic, displacements in the direction of motion are much larger than displacements in the transverse direction. In principle, experimentally this can be directly demonstrated using flux visualization techniques, such as scanning SQUID or Hall probes. With these techniques individual vortices can only be resolved at small fields. Usually statically pinned vortices are visualized after cooling in fixed magnetic field. Nevertheless it should be also possible to visualize shapes of the dynamically-pinned vortices near the boundary of the Bean profile which is formed when the magnetic field is applied after cooling of superconducting sample in zero field. We expect that the vortex field profiles to be strongly elongated along the direction of motion. The elongation length along the direction of motion is given by the longitudinal displacement u_l at the distance of the order of the London penetration depth. This length is expected to decrease with increasing temperature.

In conclusion, we developed quantitative description of individual vortex lines pinned by array of nanoparticles. We found that the critical force grows roughly as a square root of the pin density. This result is consistent with qualitative estimate assuming that for our pin-density range trapping events mostly occur as a result of direct collisions with pinning centers. The apparent critical force is strongly suppressed by thermal noise. Relative suppression reduces with increasing pin density. The configurations of pinned lines are strongly anisotropic, displacements in the drive directions are much larger than in the transverse direction. The displacement anisotropy is rapidly reduced by thermal noise mostly due to rapid reduction of the longitudinal displacements. This leads to straightening of the lines in the critical region. Analyzing behavior of the structure factors at small wave vectors, we found that the roughening index for the longitudinal displacements exceeds one. This means that the local stresses in the critical region increase with the line length indicating break down of elastic description in the thermodynamic limit. Behavior of the structure factor at large wave vectors for both directions is typical for the displacement induced by random force. At finite temperature this random-force regime is rapidly replaced by the thermal displacements.

ACKNOWLEDGMENTS

The authors would like to thank J. R. Thompson for very helpful discussions and for providing unpublished parameters of the films studied in Ref. 7. The authors also acknowledge useful discussions with D. K. Christen, L. Civale, and V. B. Geshkenbein. A.E.K. was supported by UChicago Argonne, LLC, operator of Argonne National Laboratory, a U.S. Department of Energy Office of Science laboratory, operated under contract No. DE-AC02-06CH11357. This work also was supported by the "Center for Emergent Superconductivity", an Energy Frontier Research Center funded by the U.S. Department of Energy, Office of Science, Office of Basic Energy Sciences under Award Number DE-AC0298CH1088. A.B.K acknowledges hospitality at Argonne National Laboratory and the support from CNEA, CONICET under Grant No. PIP11220090100051, and ANPCYT under Grant No. PICT2007886.

[1] L. Civale, B. Maiorov, A. Serquis, J. O. Willis, J. Y. Coulter, H. Wang, Q. X. Jia, P. N. Arendt, J. L. MacManus-Driscoll, M. P. Maley, and S. R. Foltyn, Appl. Phys.Lett., **84**, 2121(2004).

[2] T. Haugan, P. N. Barnes, R. Wheeler, F. Meisenkothen, and M. Sumption, Nature **430**, 867 (2004).

[3] X. Song, Zh. Chen, Sang-II Kim, D. M. Feldmann, D. Larbalestier, J. Reeves, Y. Xie, and V. Selvamanickam, Appl. Phys. Lett. **88**, 212508 (2006).

[4] J. Gutiérrez, A. Llordés, J. Gázquez, M. Gibert, N. Romà, S. Ricart, A. Pomar, F. Sandiumenge, N. Mestres, T. Puig, and X. Obradors, Nature Materials **6**, 367 (2007); J. Gutierrez, T. Puig, and X. Obradors, Appl. Phys. Lett. **90**, 162514 (2007).

[5] H. Yamasaki, K. Ohki, H. Yamada, Y. Nakagawa and Y. Mawatari, Supercond. Sci. Technol. **21**, 125011 (2008).

[6] M. Miura, B. Maiorov, S. A. Baily, N. Haberkorn, J. O. Willis, K. Marken, T. Izumi, Y. Shiohara, and L. Civale, Phys. Rev. B **83**, 184519 (2011).

[7] Ö. Polat, J. W. Sinclair, Y. L. Zuev, J. R. Thompson, D. K. Christen, S. W. Cook, D. Kumar, Yimin Chen, and V. Selvamanickam, Phys. Rev. B **84**, 024519 (2011). The concentration of (Y-Gd)$_2$O$_3$ precipitates in the studied (Gd-Y)Ba$_2$Cu$_3$O$_7$ films was 5×10^{16}cm^{-3} and the low-field critical current for 2.8 μm-thick film was 2.08×10^7 amp/cm^2 at 5K and 6.22×10^6 amp/cm^2 at 55k (private communication from J. R. Thompson, C. Cantoni, Ö. Polat, and D. K. Christen).

[8] J. L. MacManus-Driscoll, S. R. Foltyn, Q. X. Jia, H. Wang, A. Serquis, L. Civale, B. Maiorov, M. E. Hawley, M. P. Maley, and D. E. Peterson, Nature Materials **3**, 439 (2004); B. Maiorov, S. A. Baily, H. Zhou, O. Ugurlu, J. A. Kennison, P. C. Dowden, T. G. Holesinger, S. R. Foltyn and L. Civale, Nature Materials **8**, 398 (2009).

[9] S. Kang, A. Goyal, J. Li, A. A. Gapud, P. M. Martin, L. Heatherly, J. R. Thompson, D. K. Christen, F. A. List, M. Paranthaman, D. F. Lee, Science **311**, 1913 (2006).

[10] C. V. Varanasi, P. N. Barnes, and J. Burke, Supercond. Sci. Technol. **20**, 1071 (2007); C. V. Varanasi, J. Burke, L. Brunke, H. Wang, M. Sumption, and P. N. Barnes, J. Appl. Phys. **102**, 063909 (2007); C.V. Varanasi, J. Burke, and L. Brunke, H. Wang, J.H. Lee, and P.N. Barnes, J. Mater. Res., **23**, 3363 (2008); C. V. Varanasi, J. Burke, H. Wang, J. H. Lee, and P. N. Barnes, Appl. Phys. Lett. **93**, 092501 (2008).

[11] Yu. N. Ovchinnikov and B. I. Ivlev, Phys. Rev. B **43**, 8024 (1991).

[12] C. J. van der Beek, M. Konczykowski, A. Abal'oshev, I. Abal'osheva, P. Gierlowski, S. J. Lewandowski, M. V. Indenbom, and S. Barbanera, Phys. Rev. B **66**, 024523 (2002).

[13] A. O. Ijaduola, J. R. Thompson, R. Feenstra, D. K. Christen, A. A. Gapud, and X. Song, Phys. Rev. B **73**, 134502 (2006).

[14] C. J. van der Beek, G. Rizza, M. Konczykowski, P. Fertey, I. Monnet, Th. Klein, R. Okazaki, M. Ishikado, H. Kito, A. Iyo, H. Eisaki, S. Shamoto, M. E. Tillman, S. L. Budko, P. C. Canfield, T. Shibauchi, and Y. Matsuda, Phys. Rev. B **81**, 174517 (2010); C. J. van der Beek, M. Konczykowski, Sh. Kasahara, T. Terashima, R. Okazaki, T. Shibauchi, and Y. Matsuda, Phys. Rev. Lett. **105**, 267002 (2010).

[15] E. W. J. Straver, J. E. Hoffman, O. M. Auslaender, D. Rugar, K. A. Moler, Appl. Phys. Lett. **93**, 172514 (2008); O. M. Auslaender, L. Luan, E. W. J. Straver, J. E. Hoffman, N. C. Koshnick, E. Zeldov, D. A. Bonn, R. Liang, W. N. Hardy, K. A. Moler Nature Physics, **5**, 35(2009); C. Reichhardt, Nature Physics **5**, 15 (2009).

[16] This formula is valid only for the case $b \gg \xi_{ab}$. When b is comparable with ξ_{ab}, interpolation $\mathcal{L}_p \approx (1/2)\ln[1+(b/\xi_{ab})^2]$ should be used.

[17] The cutoff lengths $r_{\max}$ and $r_{\min}$ depend on microscopic details. Typically, $r_{\max}$ is determined by the length scale of line deformation in the z direction, which in our case is given by the trapping length L_t. The lower bound for $r_{\min}$ is given by the c-axis coherence length ξ_c. However, in layered superconductors more accurately $r_{\min}$ can be estimated as the typical distance between the pancake vortices in the neighboring layers devided by the anisotropy factor γ.

[18] G. Blatter, V. B. Geshkenbein, and J. A. G. Koopmann, Phys. Rev. Lett. **92**, 067009 (2004).

[19] Near depinning threshold, the pin-vortex potential as a function of the pinned-point displacement u can be expanded as $V(u) = (F_p - F)(u - u_c) - (b/6)(u - u_c)^3$ where $F \approx fL_t$ and $u = u_c$ is the marginal equilibrium point. Below threshold this yields the barrier $U(F) = [4\sqrt{2}/(3\sqrt{b})](F_p - F)^{3/2}$.

[20] P. Le Doussal, and K. J. Wiese, Europhys. Lett. **77**, 66001 (2007); A. Rosso, P. Le Doussal, and K. J. Wiese, Phys. Rev. B **75**, 220201(R) (2007).

[21] See EPAPS document No. XXXXXXX for animation of the line motion through array of the strong pins.

[22] D. Ertaş, and M. Kardar, Phys. Rev. B **53**, 3520 (1996).

[23] H. Leschhorn and Lei-Han Tang Phys. Rev. Lett. 70, 2973 (1993).

[24] A. Rosso, A. K. Hartmann, and W. Krauth, Phys. Rev. E **67**, 021602 (2003).

[25] C. J. Bolech and A. Rosso, Phys. Rev. Lett. **93**, 125701 (2004).

[26] A. B. Kolton, A. Rosso, E. V. Albano, and T. Giamarchi, Phys. Rev. B **74**, 140201(R) (2006).

[27] T. Nattermann, S. Stepanow, L.-H. Tang, and H. Leschhorn, J. Phys. II **2**, 1483 (1992); O. Narayan and D.S. Fisher, Phys. Rev. B **48**, 7030 (1993).